Desynchronization of cerebellar Purkinje cell population activity during postnatal development

（生後発達期における小脳プルキンエ細胞集団活動の非同期化）

グッド ジャンマルク

Good Jean-Marc

Table of contents

Abstract

The inferior olive of the medulla oblongata sends glutamatergic afferents to the cerebellum. In adult rodents, axons of inferior olivary neurons divide into several climbing fibers (CFs) that innervate cerebellar Purkinje cells (PCs) in a one-to-one manner. Activation of CFs generates bursts of action potentials known as complex spikes (CSs) in PCs. CSs in neighboring PCs are synchronized due to electrical coupling between inferior olivary neurons. During early postnatal period, however, the pattern of CS activity in populations of PCs remains unclear. CF-PC synapses undergo dynamic changes during the first two postnatal weeks including selective strengthening of a single CF and elimination of redundant CFs in each PC. In this study, I used *in vivo* two-photon calcium imaging to monitor CS activity from populations of PCs during the period of the CF network refinement. I found that CS activity was highly correlated among neighboring PCs in newborn mice and progressively desynchronized during the first postnatal week. The degree of synchrony declined to the adult level at postnatal day 8. I also analyzed PC-specific $Ca_v2.1$ knockout mouse, in which selective strengthening of a single CF and elimination of redundant CFs in each PC is impaired. The progressive desynchronization of CS activity observed in wild-type mice was incomplete in the knockout mice. These results suggest that the configuration of the CF

network has a direct impact on the pattern of CS activity in PC populations and that the desynchronization of CS activity might result from the CF network refinement.

Introduction

Electrical activity in developing central nervous system

During the development of the central nervous system, neuronal networks exhibit specific patterns of spontaneous activity. This activity is considered to control processes of neuronal differentiation [1], migration and axon guidance [2, 3], synaptogenesis and synaptic refinement [4, 5]. One of the best studied examples is the formation of eye-specific layers in the lateral geniculate nucleus for which spontaneous correlated waves of action potential in retinal ganglion cells are critical [4, 6-8]. In the cerebellum, the migration of granule cells was shown to be regulated by calcium influx through voltage and ligand-gated channels [9].

The mechanisms mediating the spontaneous activity in immature neural circuits are very diverse and highly dependent on the brain region [10]. Neocortical oscillations, for example, are dependent on glutamatergic synaptic transmission through ionotropic [11] and metabotropic [12] receptors, while in the hippocampus, GABAergic synaptic transmission is required to generate bursts of spontaneous activity [13, 14].

In spite of this diversity, early patterns of electrical activity share common features. Notably, many of them exhibit a high synchrony among populations of neurons [15]. This was described *in vitro* in various regions of the central nervous system

including neocortex [11], hippocampus [14, 16] , spinal cord [17] and retina [18]. More recently, two-photon calcium imaging enabled to examine this correlated pattern of activity *in vivo* with a single-cell resolution. For example, in barrel cortex of new born mice, the activity in populations of layer 2/3 neurons is highly coordinated and undergoes a desynchronization at the end of the second postnatal week [19]. Similarly, in the visual cortex, the fraction of simultaneously active neurons is high in early postnatal days and drops dramatically after eye-opening [20].

The mechanisms responsible for the synchronization of neuronal activity are thought to change along with the development. In new born animals, populations of neocortical neurons are coactive due to electrical coupling by gap junctions [21, 22], whereas at the end of the first postnatal week, cortical synchronized oscillatory activity was shown to be mediated by chemical synaptic transmission acting through NMDA receptors [22]. However, the circuit mechanisms of synchronization are still not completely understood.

The olivocerebellar system

The inferior olivary nucleus constitutes one of the two major glutamatergic afferent systems to the cerebellum [23]. In adult rodents, axons of olivary neurons divide into several climbing fibers (CFs) [24] that innervate cerebellar Purkinje cells (PCs) in a

one-to-one manner. The activation of CF-PC synapse generates a burst of action potentials known as complex spike (CS) [25], which triggers a widespread influx of calcium into PCs [26]. PCs exhibit another type of spike activity, termed simple spike (SS), which is due to intrinsic membrane properties of PCs [27]. SS firing pattern is modulated by excitatory inputs from parallel fibers, the axons of granule cells, and inhibitory inputs from stellate cells and basket cells [28, 29]. The presence of electrotonic coupling by gap junctions between olivary neurons [30] is responsible for the synchronization of spontaneous CSs in nearby PCs [31, 32]. This synchrony is especially obvious between nearby PCs located within rostro-caudally oriented bands called microzones (3 to 19 dendritic arbor wide), and tends to fall off more sharply in the medio-lateral direction [33-35]. The level of synchrony is regulated by the activity of GABAergic and glutamatergic afferents to the inferior olive, which respectively decrease and increase the coupling between olivary neurons [36-38].

Refinement of CF-PC synapses during postnatal development

During the postnatal period, CF-PC synapses undergo several dynamic changes that have been characterized by electrophysiological recordings. At birth each PC soma is innervated by several CFs, and during the first postnatal week, only one CF on each PC

soma is selectively strengthened relatively to the others in a process called functional differentiation [39]. During the subsequent period, weak CFs are eliminated while the strong CF translocates to PC dendrite [40]. These findings are supported by a morphological study in which the trajectory of single olivary axons were reconstructed [41]. This study shows that soon after birth, each CF has collaterals making weak contacts with several PCs, a stage called “creeper” type terminal arbor [42], and that during the first postnatal week, the innervation territory of single CFs will contract to form a “nest” type terminal arbor [43], characterized by dense aggregations of terminals tightly surrounding single PC somata.

Purpose and focus of the research

In the olivocerebellar system, remodeling of CF-PC synapses is thought to be closely related to the pattern of activity in PCs during early postnatal period [44-48]. However, this activity has never been described *in vivo* at a population level. In this study, by using two-photon calcium imaging in living mice, spontaneous CF responses in populations of PCs were investigated during the period of CF network refinement. I found that the CS activity was highly correlated among neighboring PCs in newborn mice and progressively desynchronized at the end of the first postnatal week. I also

performed the same analysis in PC-specific $Ca_v2.1$ knockout (PC-Cav2.1 KO) mouse, in which the functional differentiation of multiple CFs, dendritic translocation of a single CF, and elimination of weaker CFs are impaired in each PC [49]. I found that the desynchronization of CS activity observed in wild-type (WT) mice was incomplete in PC-Cav2.1 KO mice. These results suggest that CS activity patterns in PC populations are highly dependent on CF-PC synaptic wiring and the desynchronization of CS activity results, at least in part, from the CF network refinement.

Materials and Methods

Animals

In the first part, C57Bl/6N WT mice from postnatal day (P) 3 to P24 (mice were considered adult after P21 [50]) were used. For the second part, PC-Ca_v2.1 KO mice produced as previously described [49] were used. PC-Ca_v2.1 KO mice (Ca_v2.1lox/lox, GluD2+/Cre) were compared with their littermates carrying the floxed Ca_v2.1 gene but no Cre gene (Cav2.1lox/lox, GluD2+/+). All procedures including animal care were approved by the University of Tokyo Animal Care and Use committee (Approval number: P08-015).

Cranial window surgery

Animals were put on a warm blanket and anesthetized with 1-3% isoflurane. The depth of anesthesia was constantly monitored by observing pinch withdrawal reflex of forelimb. The skin and muscles were removed and a metal plate was fixed with dental acrylic cement over the lobule 4-6 of the cerebellar vermis. A ~2mm craniotomy was performed and the dura mater was carefully removed. 1.5% agarose was mounted over the craniotomy and a glass coverslip was held in place with metal clips on the top to reduce motion artifacts due to respiration and heartbeat [35, 51].

Labeling Procedure

All the procedure was described previously [51] and followed with partial modifications. 50μg Oregon Green BAPTA-1 AM (OGB-1, Invitrogen), a membrane permeable calcium sensitive indicator, was dissolved into Pluronic F-127 (Molecular Probes) in DMSO (Sigma) [52]. The resulting solution was ~25-fold diluted into a solution containing (in mM) 150 NaCl, 2.5 KCl, 1 $MgCl_2$, 2 $CaCl_2$, 10 HEPES, pH 7.3 (final concentration of OGB-1 is ~0.2-0.3 mM). 0.02 mM Alexa 594 (Invitrogen) was added for better visualization during the injection. A thin glass pipette (5-6 MΩ) was inserted into the molecular layer of the cerebellar cortex and the calcium indicator solution injected with a positive pressure of ~0.5 bar during 1~3 minutes (Picospritzer; General Valve). Calcium imaging was performed after diffusion of the dye into the intracellular compartment, approximately from 45 minutes post-injection.

Two-photon calcium imaging

In vivo two-photon imaging was performed using a custom two-photon microscope (Sutter Instruments). Images were acquired using ScanImage software [53] written in MATLAB (MathWorks). Laser power was maintained <20 mW at the sample.

Horizontal full frame scan movies were recorded with a 40x objective lens (Olympus). Since the dendrites of PCs are still immature during the early postnatal period, recordings were performed from the PC somata until P10 unless otherwise mentioned. In older animals, calcium signals obtained from PC somata were too weak to detect, and therefore calcium signals were recorded from the PC dendrites in the molecular layer. The duration and acquisition speed were modified in function of the postnatal age to better fit the frequency and kinetics of calcium transients. Typically, in P10 to P24 mice, 64-128 s movies were obtained at 15.6 Hz while in P3 to P12 mice, the acquisition frequency was 7.8 or 3.9 Hz and the duration of the movies 256-512 s.

Calcium imaging analysis and CSs firing rate reconstruction

In every full frame scan movie, several regions of interest corresponding to PC somata or dendrites were randomly selected on Image J. The non-overlapping arrangement of PC arbors allowed a single cell resolution at both recording locations [35]. The average fluorescence values for every region of interest were calculated at each time point and expressed as relative fluorescence changes $\Delta F/F$ after background subtraction. The rest of the analysis was performed with Igor Pro (wavemetrics). Each $\Delta F/F$ trace was low-pass filtered using a Butterworth filter with a cutoff frequency of 0.5 Hz for

recording at P3-12 and 1.2 Hz in P21-24 mice to preserve the shape of short duration transients. Then, every ΔF/F trace was deconvolved with a 2 s single-exponential kernel using routines custom-written in MATLAB [19, 54]. The standard deviation of all the points below zero was calculated, multiplied by four, and set as a threshold below which all points of the deconvolved trace were set to zero [19]. Reconstructed CSs firing rates were finally obtained by multiplying the deconvolved traces with a scaling factor (61.3 ± 11.8 n=8 cells). All the parameters of the reconstructions were empirically determined by cell-attached recordings performed simultaneously to calcium imaging in WT mice (P8-24). The CS firing rates extracted from the electrophysiological recordings (actual CS firing rates) were expressed with a Gaussian kernel.

This reconstruction technique is based on the assumption that each CS generates a unitary calcium transient characterized by an exponential decay. It is hence possible to approximate calcium fluctuations in function of the CS firing pattern. This can be done by a temporal convolution of the time series of CSs with an exponential kernel. Conversely, the train of CSs can be reconstructed from the calcium fluctuations by the inverse operation called temporal deconvolution with an exponential kernel.

Evaluation of synchrony

Correlation coefficients were calculated between every pair of deconvolved calcium traces from nearby PCs by normalizing cross-correlation to auto-correlation at zero lag time. This is expressed by the formula: $(A*B)/\sqrt{\text{norm}A * \text{norm}B}$, where A and B represent deconvolved calcium vectors from each PC while norm means the Euclidean length. The mean correlation coefficients were calculated for every animal and, in turn, an average value was calculated between all the animals of a given age group or genotype. To determine whether measured correlation coefficients were significantly higher than chance level, 100 surrogate deconvolved calcium traces with randomly shifted events times were generated for every trace. Cell pairs with a correlation coefficient greater than the 95th percentile of correlation coefficients in the randomized samples were considered statistically significant [19, 55].

Evaluation of frequency and half width

To evaluate the frequency of spontaneous calcium transients, the standard deviation was calculated for every $\Delta F/F$ trace, multiplied by two, and set as a threshold for detection. For the half width calculation, the baseline and peak level were determined manually for all calcium transients. The duration at the half-height level was then measured and

averaged.

Cell-attached recordings

In vivo extracellular loose cell-attached recordings were performed to monitor the spiking activity of PCs. Patch electrodes with final resistance of 4-6 MΩ were prepared from glass capillaries with a multi-stage puller (Sutter). They were filled with solution containing (in mM): 150 NaCl, 2.5 KCl, 10 HEPES, 2 $CaCl_2$, 1 $MgCl_2$ and 0.05 Alexa-594 to visualize and target PCs [56]. A Multiclamp 700B amplifier (Molecular Devices) was used, and the data were acquired with a DigiData 1322 (Axon Instruments) at 20 kHz and low-pass filtered at 10 kHz. After the recording, the cells were labeled with Alexa-594 by current injection (-30 nA) to facilitate their identification. The CSs were distinguished from SSs based on their characteristic shape.

Morphological analysis

For anterograde labeling of CFs, mice at P7 were anesthetized by ether and dextran Alexa-594 (DA-594; Invitrogen) was injected into the inferior olive by dorsal approach as described in [57]. After three days (at P10), mice were transcardially perfused with 4% paraformaldehyde in 0.1 M sodium phosphate buffer and processed for parasagittal

microslicer sections (50 μm in thickness; VT1000S; Leica). For triple fluorescent labeling, goat calbindin antibody (1 μg/ mL a marker of PCs) and vesicular glutamate transporter 2 (VGluT2, a marker of CF terminals) antibody (0.5 μg/mL) were used as previously reported [58, 59]. Cerebellar sections were incubated with 10% normal donkey serum for 20 min, a mixture of primary antibodies overnight, and a mixture of Alexa Fluor 488- (Invitrogen) and indocarbocyanine (Cy3) (Jackson Immunoresearch)-labeled species-specific secondary antibodies for 2 h at a dilution of 1:200. All immunohistochemical incubations were done at room temperature in a free-floating state. Single-plane images were taken with a confocal laser scanning microscope (FV1000; Olympus) and analyzed with Metamorph software (Universal Imaging). The quantitative analysis focused on the following two parameters. (1) The length of CF collaterals that was defined as the horizontal distance between the bifurcation point from the main branch and the corresponding terminal tip. (2) The number of terminals per collateral that was evaluated by counting the number of VGluT2-positive puncta per collateral on PCs.

Statistical analysis

All statistical values were presented as mean±SEM. Mann-Whitney U test was used to

compare two independent sets of data. One-way analysis of variance (ANOVA) tests with Holm-Sidak post-hoc analysis were performed for the comparison of several groups. Difference between groups were judged significant for $p<0.05$.

Results

Properties of spontaneous calcium transients in postnatal cerebellar PCs

The fluorescent calcium indicator Oregon Green 488 BAPTA-1/AM (OGB-1) was bulk loaded into the cerebellar cortex of anesthetized young WT mice, and spontaneous activity in PCs was monitored by *in vivo* two-photon calcium imaging (Fig. 1). The developmental profile of calcium transients was first analyzed in single PCs. Their mean frequency gradually increased during the first three postnatal weeks: P3-P5: 0.01 ±0.003 Hz, 6 mice; P6-P7: 0.03±0.005 Hz, 12 mice; P8-12: 0.08±0.02 Hz, 12 mice; P21-24: 0.36±0.04, 8 mice (Fig. 2A, B). In contrast, the average half width was largest in newborn animals, and gradually decreased along with the postnatal development: P3-P5: 9.65±2.00 s, 6 mice; P6-P7: 6.30±1.00 s, 12 mice; P8-12: 2.24±0.17 s, 12 mice; P21-24: 0.92±0.09 s, 8 mice (Fig. 2A, C).

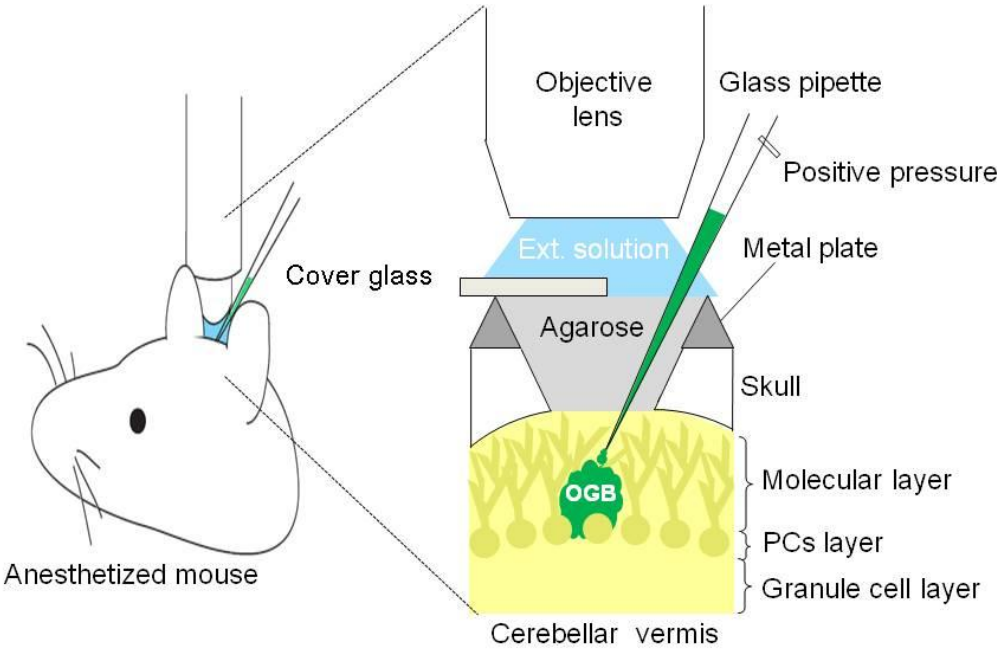

Figure 1

Bulk loading of calcium indicator and *in vivo* two-photon monitoring of cerebellar PC population activity.

A metal plate was fixed on the skull of an anesthetized mouse over the cerebellar vermis, and a craniotomy was performed. OGB-1 was pressure ejected into the molecular layer of the cerebellar cortex with a thin glass pipette. After penetration of the dye into the intracellular compartment, PC population activity was monitored with a two-photon microscope at single cell resolution.

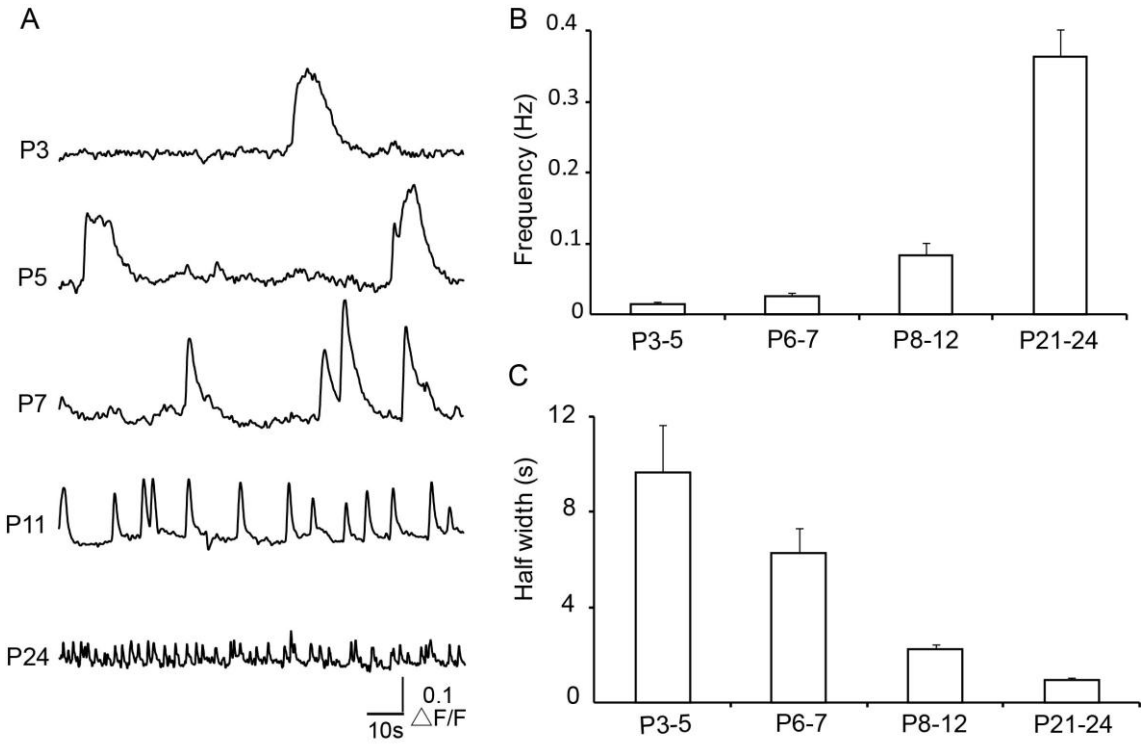

Figure 2

Properties of spontaneous calcium transients in individual PCs during postnatal development.

(A) Representative traces of calcium transients obtained from single PCs at indicated mouse ages. (B, C) Average frequency (B) and half-width (C) of calcium transients at four developmental stages.

In adult rodents, calcium transients in PCs are known to reliably match CS activity [35, 60]. To investigate the nature of the spontaneous calcium transients in young animals, cell-attached unit recordings were performed simultaneously with calcium imaging in WT mice from P8 to P24 (Fig. 3). Similarly to the results of adult mice, I found that calcium transients exclusively reflected the occurrence of CF responses in young mice (Fig. 3A-H). In contrast, SSs did not generate any detectable calcium increase. Then, I used an established temporal deconvolution algorithm to reconstruct CS firing rates from changes in the fluorescence signal [19, 54]. The correlation between the reconstructed CS firing rates and actual CS firing rates obtained from electrophysiological recordings was high (correlation coefficient: 0.85±0.02, 8 cells) (Fig. 3A-H). Also with this technique, 96±2.9% of the single CSs and 100% of a succession of two or more CSs (Fig. 3I) could be detected. These results confirm the reliability of the reconstruction.

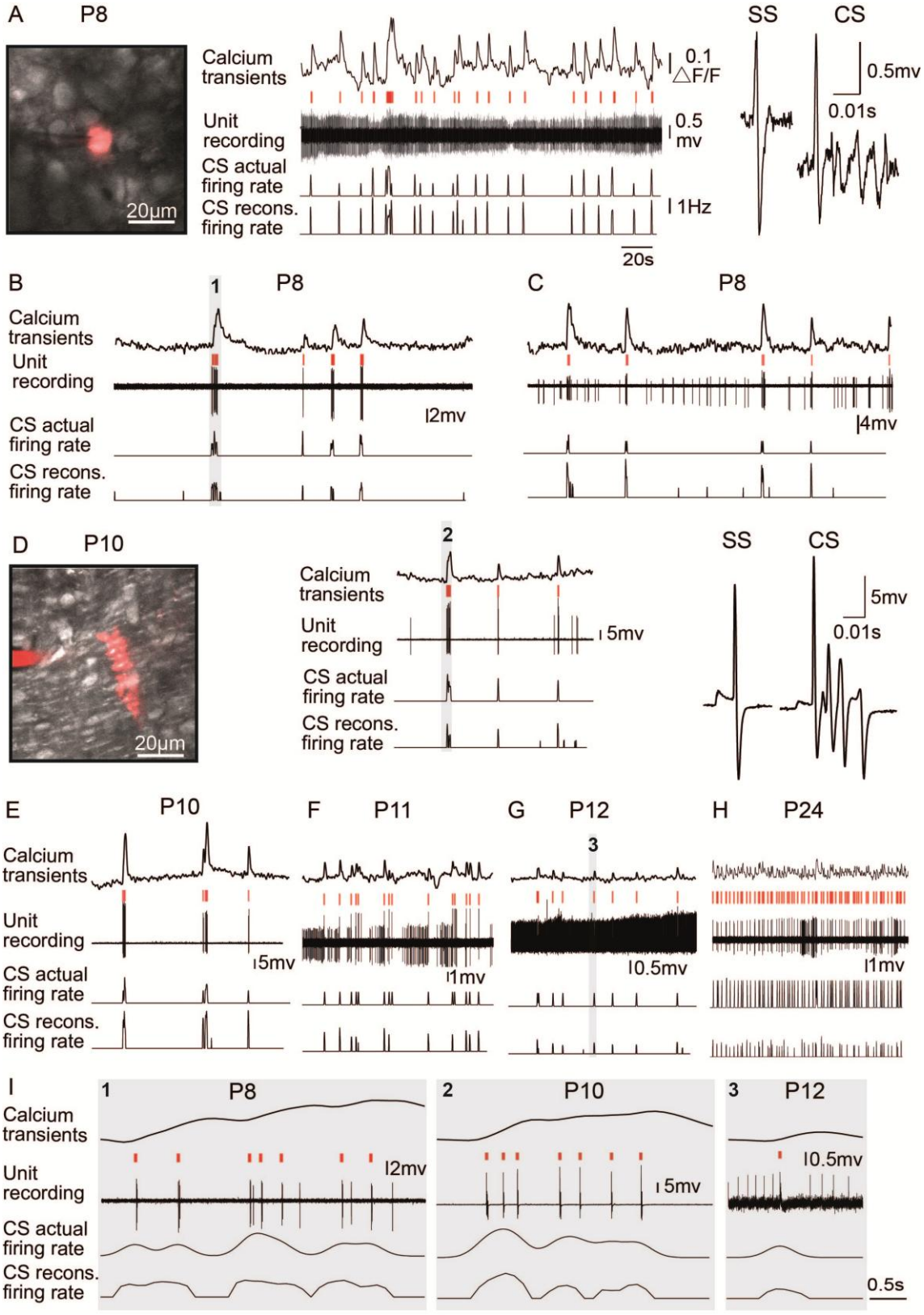
A
P8
20μm
Calcium transients
Unit recording
CS actual firing rate
CS recons. firing rate
0.1 △F/F
0.5 mv
1Hz
20s
SS
CS
0.5mv
0.01s
B
P8
1
Calcium transients
Unit recording
CS actual firing rate
CS recons. firing rate
2mv
C
P8
4mv
D
P10
20μm
2
Calcium transients
Unit recording
CS actual firing rate
CS recons. firing rate
5mv
SS
CS
5mv
0.01s
E
P10
Calcium transients
Unit recording
CS actual firing rate
CS recons. firing rate
5mv
F
P11
1mv
G
P12
3
0.5mv
H
P24
1mv
I
1
P8
2mv
2
P10
5mv
3
P12
0.5mv
0.5s

Figure 3

Reconstruction of CS firing rates from calcium transients in PCs.

Somatic unit recordings and calcium imaging performed simultaneously in PC somata at P8 (A-C) and dendrites at P10, P11, P12 and P24 (D-H) in WT mice. (A-H) The CS actual firing rates are derived from unit recordings while CS reconstructed firing rates are obtained by deconvolution of calcium transients [19, 54]. CSs are marked with red strokes. (A, D left) Labeling of PCs with Alexa for identification of recorded PCs. (A, D right) Enlargement of representative SSs and CSs from the corresponding unit recordings showing their characteristic shapes. (I) Enlargement of three regions (in grey) from B, D and G at P8, P10 and P12 respectively.

Developmental desynchronization of PCs population activity

In this part, I focused on the spatiotemporal pattern of activity in a population of PCs during the postnatal development. Calcium transients were extracted (Fig. 4B, 5B) from several randomly selected regions of interest corresponding to single PC somata (Fig. 4A) or dendrites (Fig. 5A). Then, CS firing rates were reconstructed for each cell (Fig. 4C, 5C). At P5, calcium transients recruited large clusters of PCs while the activity became progressively more decorrelated with age (P7, P8, P10) (Fig. 4B-C, 5B-C). To describe this phenomenon, I estimated the level of synchrony in population of PCs by calculating pairwise correlation coefficients between deconvolved calcium traces. In Fig. 4D and Fig. 5D, the correlation coefficients between all possible cell pairs were expressed in matrices and displayed with a color scale for every age group. An overall decrease in synchrony could be observed during the first postnatal week.

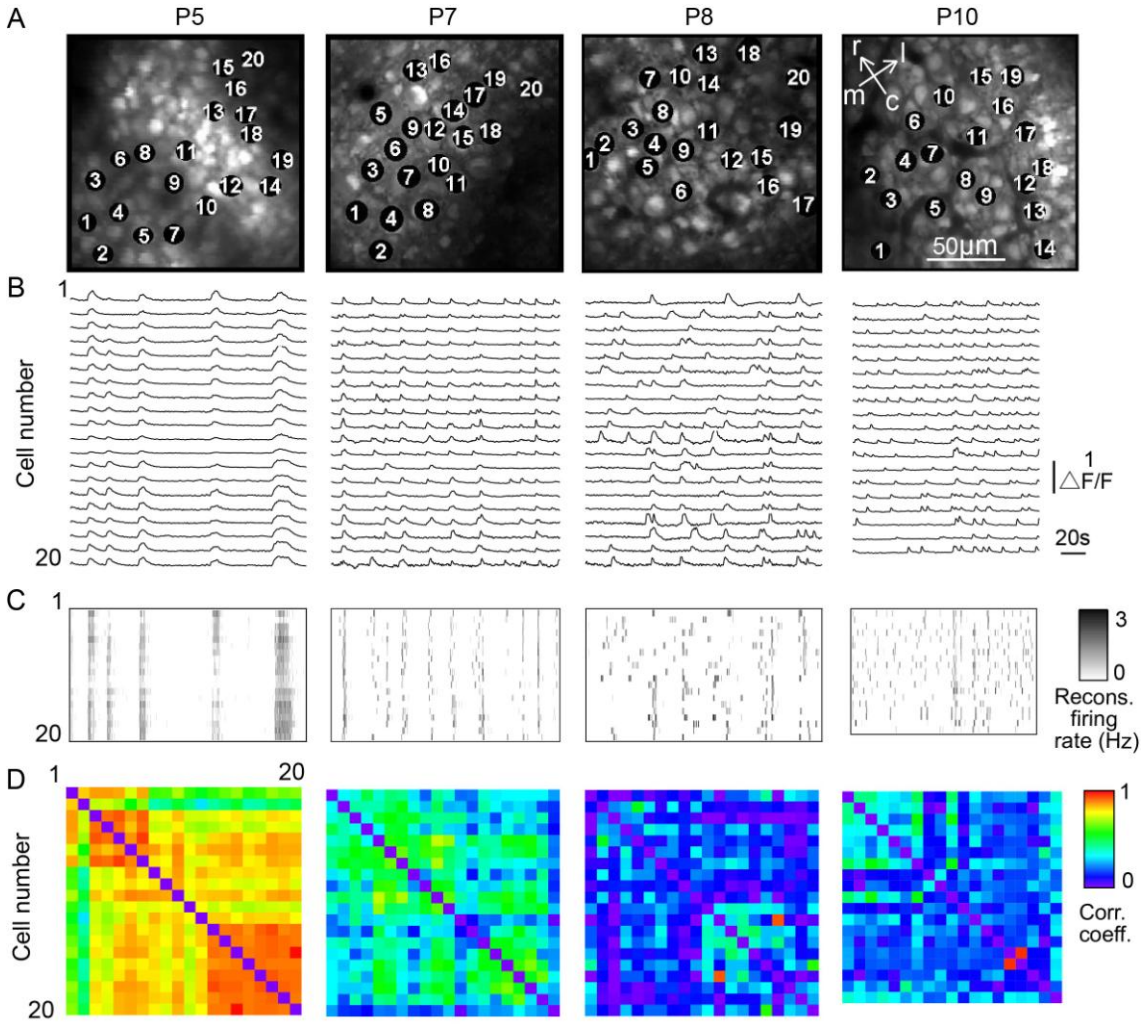

Figure 4

CF responses in populations of PCs during early postnatal days.

(A) Full frame scan movies were recorded at the PC layer. 19 to 20 regions of interest (black discs) corresponding to single PC somata were numbered (in white) following rostral to caudal and then medial to lateral order. (B) Calcium transients were obtained by extracting relative fluorescence changes from each region of interest. (C) Reconstructed CS firing rates were derived from temporal deconvolution of calcium transients traces. (D) Matrices displaying correlation coefficients between the deconvolved calcium traces of all possible pairs.

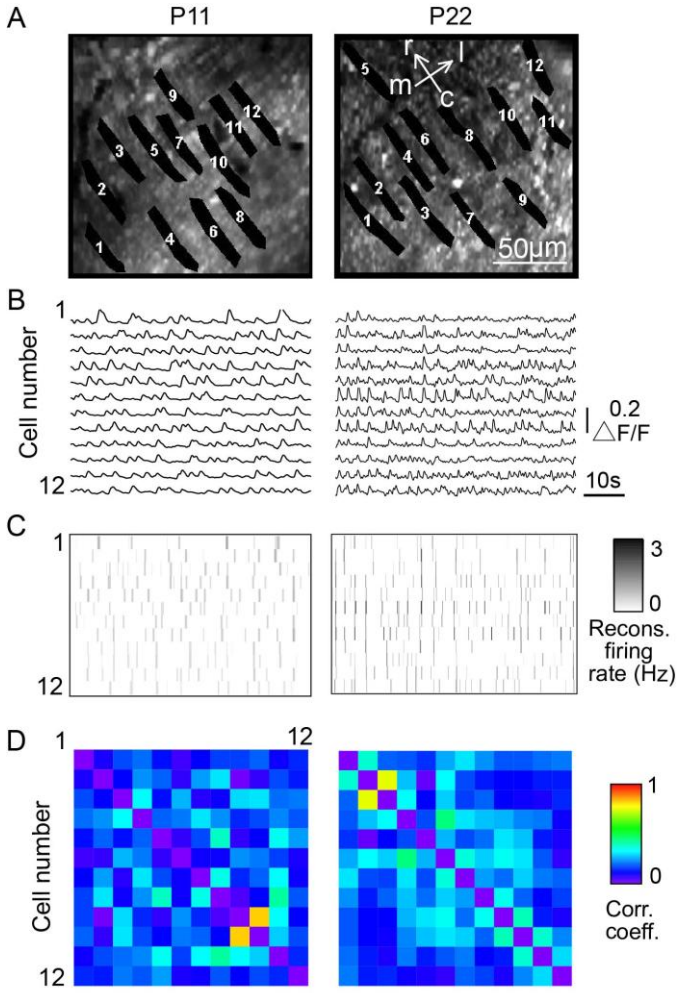

Figure 5

CF responses in populations of PCs at later developmental stages.

(A) Full frame scan movies were recorded in molecular layer. 12 regions of interest (in black) corresponding to individual PC dendrites were numbered (in white) following rostral to caudal and then medial to lateral order. (B) Calcium transients were obtained by extracting relative fluorescence fluctuations from each region of interest. (C) Reconstructed firing rates were derived from temporal deconvolution of calcium transients traces. (D) Matrices displaying correlation coefficients between the deconvolved calcium traces of all possible pairs.

To better characterize this developmental desynchronization of PC population activity, pairwise correlation coefficients obtained from several mice were averaged and plotted against the medio-lateral (Fig. 6A left) or rostro-caudal (Fig. 6A right) distance separating each pair of cells. The dependency of the synchrony to the cell separation was first analyzed by comparing mean correlation coefficient values of close (0-40 μm) and distant (80-120 μm) pairs in the medio-lateral direction. The level of synchrony tended to decrease with the medio-lateral separation. (P3-5) (0-40 μm: 0.83±0.02; 80-120 μm: 0.76±0.03, 6 mice, p=0.07, Mann-Whitney U test), (P6-7) (0-40 μm: 0.58 ±0.09; 80-120 μm: 0.38±0.10, 12 mice, p=0.15), (P8-12) (0-40 μm: 0.31±0.03; 80-120μm: 0.20±0.03, 12 mice, p=0.01), (P21-24) (0-40 μm: 0.29±0.02; 80-120 μm: 0.24±0.02, 8 mice, p=0.16). In the rostro-caudal direction, the dependency to the separation was less clear. (P3-5) (0-40 μm: 0.80±0.02; 80-120 μm: 0.81±0.02, p=0.93), (P6-7) (0-40 μm: 0.54±0.09; 80-120 μm: 0.46±0.09, p=0.37), (P8-12) (0-40 μm: 0.26±0.03; 80-120μm: 0.24±0.04, p=0.59). Next, I evaluated the developmental desynchronization of PC population activity. There was a significant difference between mean correlation coefficients at P3-5 and those of the other ages (P3-5: 0.80±0.01, 6 mice; P6-7: 0.53±0.09, 12 mice, p<0.01; P8-12: 0.25±0.03, 12 mice, p<0.001; P21-24: 0.28±0.02, 8 mice, p<0.001, One-way ANOVA followed by Holm-Sidak's

post hoc test) (Fig. 6B left). In contrast, mean correlation coefficients at P8-12 were not statistically different from those obtained at P21-24 (p=0.69). To avoid the influence of cell separation on the correlation coefficient values, the same statistical analysis was also performed individually for pairs with close (0-40 μm) and distant (80-120 μm) medio-lateral separations. In both groups the desynchronization of CS activity was significant (0-40 μm) (P3-5: 0.83±0.02; P6-7: 0.58±0.09, p=0.01; P8-12: 0.31±0.03, p<0.001; P21-24: 0.29±0.02, p<0.001) (Fig. 6B middle), (80-120 μm) (P3-5: 0.76± 0.03; P6-7: 0.38±0.10, p<0.001; P8-12: 0.20±0.03, p<0.001; P21-24: 0.24±0.02, p<0.001) (Fig. 6B right). In contrast, there wasn't any significant difference between P8-12 and P21-24 group (0-40 μm) (p=0.87), (80-120 μm) (p=0.68). Taken together, these data show that CF responses are highly correlated soon after birth, and undergo a uniform desynchronization from P5 to P8 at all separations. In addition, at almost all ages, the level of synchrony seemed to fall off more sharply in the medio-lateral direction than in the rostro-caudal direction. The statistical significance of this tendency needs however to be confirmed by analyzing population activity over a wider range of separations.

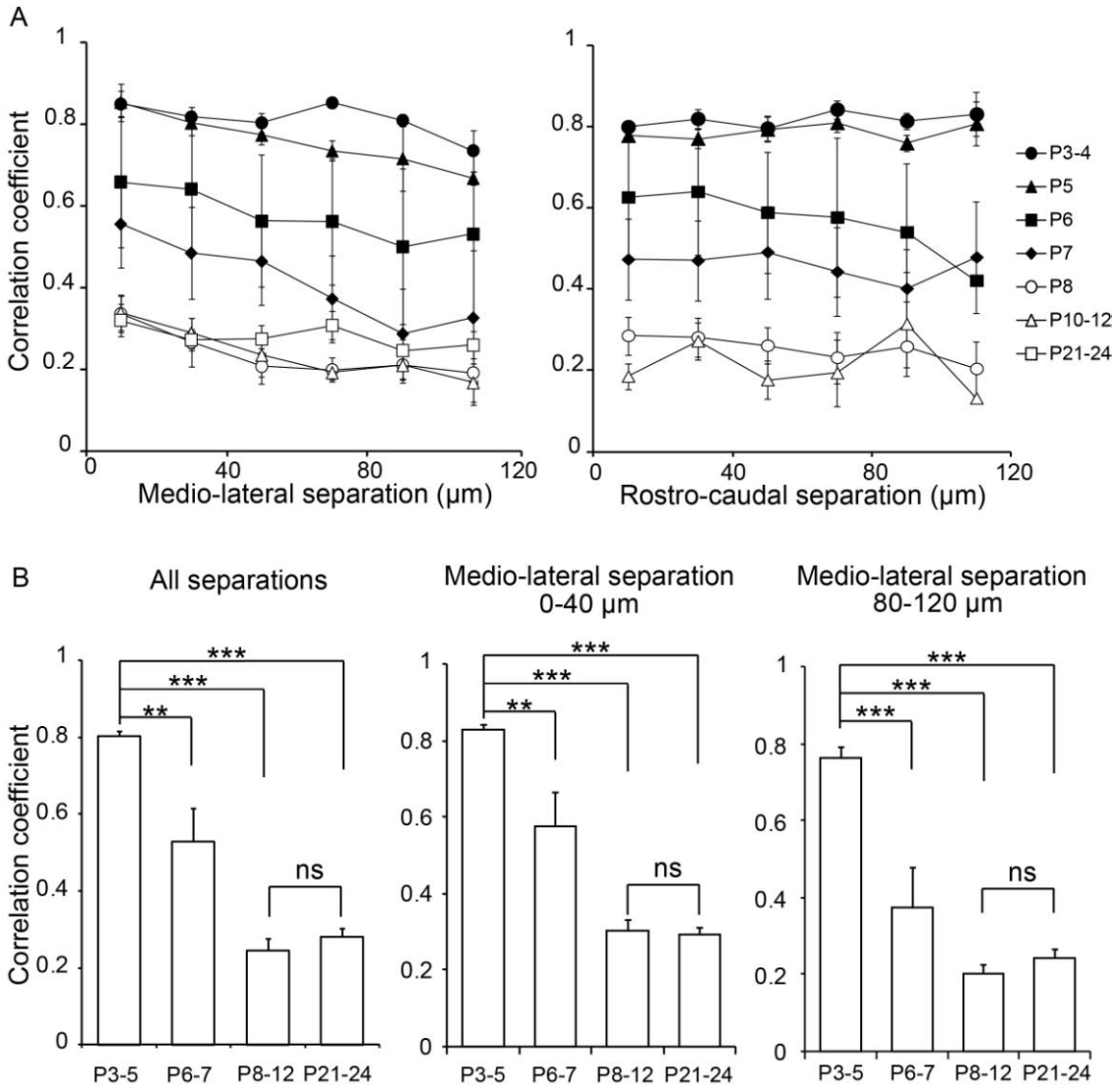

Figure 6

Developmental decline in correlation of PC population activity.

Mean correlation coefficients between deconvolved calcium traces from pairs of PCs plotted against the medio-lateral (A left) and rostro-caudal (A right) separation. P3-4: 4 mice, 246 pairs; P5: 2 mice, 166 pairs; P6: 5 mice, 273 pairs; P7: 7 mice, 326 pairs; P8: 5 mice, 848 pairs; P10-12: 7 mice, 177 pairs (medio-lateral); 5 mice, 124 pairs (rostro-caudal); P21-24: 8 mice, 154 pairs (medio-lateral). Note that rostro-caudal separation couldn't be measured at P21-24 as recordings were obtained exclusively from dendrites. (C) Averaged correlation coefficients for all data (left), medio-lateral separations of 0-40μm (middle) and 80-120μm (right). Asterisks demonstrate statistical significance between the values at P3-5 and those at one of the other ages. One-way ANOVA followed by Holm-Sidak's post hoc test.

Finally, to verify that the level of synchrony was not influenced by the location of the recording, I compared mean correlation coefficients obtained at somatic and dendritic levels in P8-P12 mice (Fig. 7). In this age group, recordings could be performed at both locations (Fig. 7A). There was no significant difference between the data recorded from the soma and dendrite at either short medio-lateral separations (0-40μm) (soma: 0.27±0.03; dendrite: 0.30±0.03 p=0.53, Mann-Whitney U test) or larger medio-lateral separations (80-120μm) (soma: 0.17±0.03; dendrite: 0.17±0.03 p=0.89) (Fig. 7B), indicating that recording locations did not influence the level of synchrony.

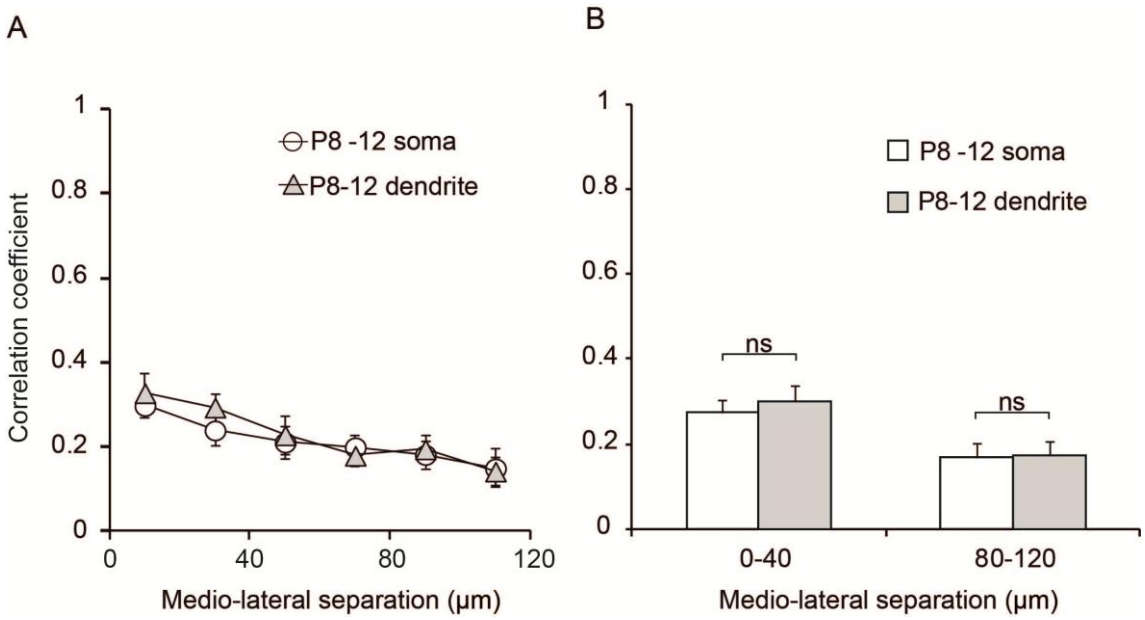

Figure 7

The level of synchrony is not influenced by the location of the recording.

(A) Mean correlation coefficients between deconvolved calcium transients recorded at somatic (10 mice, 972 pairs) and dendritic (10 mice, 238 pairs) level in P8-12 WT mice. (B) Averaged correlation coefficients for cell pairs with separation of 0-40µm (left) and 80-120µm (right) obtained from recordings at the soma and dendrite. There is no significant difference between the data from the two recording locations. Mann-Whitney U test.

Impaired desynchronization of PC population activity in PC-specific Ca_v 2.1 knockout mouse

To address whether the developmental desynchronization of cerebellar activity is related to the CF network refinement, I analyzed PC population activity in PC-specific Ca_v 2.1 knockout (PC-Ca_v 2.1 KO) mouse. In this knockout (KO) mouse, the functional differentiation of multiple CFs, dendritic translocation of a single CF, and elimination of weaker CFs are impaired in each PC, while the gross anatomy of the cerebellum and the morphology of PCs are thought to be otherwise normal [49]. It is hence a useful model to assess the influence of the dynamic changes at CF-PC synapse on the pattern of population activity.

CF responses were first observed at P4-P5. In this age group, calcium transients regrouped large clusters of PCs and the overall synchrony was high in both genotypes. Later in the development, at P9-10, the level of synchrony decreased dramatically in control mice whereas the desynchronization was incomplete in PC-Ca_v 2.1 KO mice (Fig.8 A-C). In particular, CS activities of nearby PCs remained highly correlated in PC-Ca_v 2.1 KO mice.

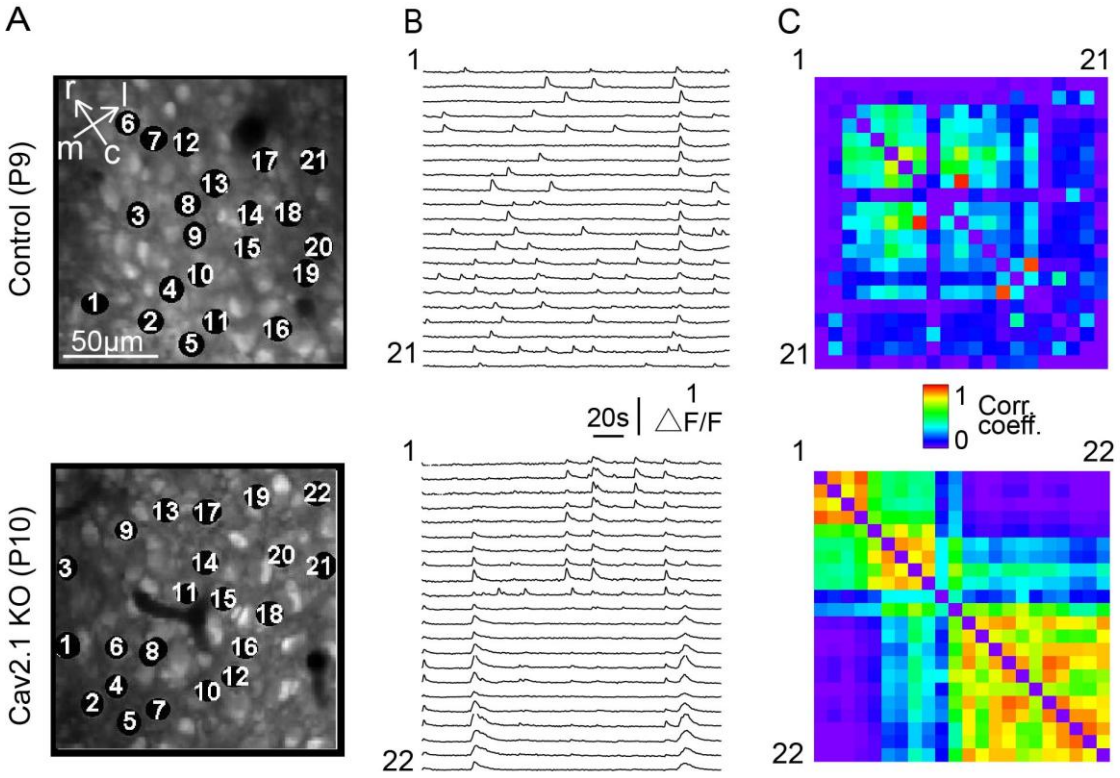

Figure 8

Developmental profile of PC population activity in PC-Ca_v 2.1 KO mouse.

(A) Full frame scan movies were recorded in PC-Ca_v 2.1 KO and control littermates at P9-10. 21 to 22 regions of interest (black discs) corresponding to PC soma were numbered (in white) following rostral to caudal and then medial to lateral order. (B) Corresponding calcium transients were obtained by extracting relative fluorescence changes from each region of interest. (D) Matrices displaying correlation coefficients between the deconvolved calcium traces of all possible pairs.

To further examine the spatiotemporal pattern of activity in PC-Ca_v 2.1 KO mice, mean correlation coefficients were plotted against the medio-lateral (Fig. 9A left) and rostro-caudal (Fig. 9A right) distance separating each pair of cells. The dependency of the synchrony to the cell separation was first analyzed by comparing mean correlation coefficient values of close (0-40 μm) and distant (80-120 μm) pairs in the medio-lateral direction. The level of synchrony tended to fall off with the medio-lateral separation in both genotypes and age groups (P4-5, P9-10). This tendency was especially clear in PC-Ca_v 2.1 KO mice at P9-10. (P4-5, Control) (0-40 μm: 0.80±0.04; 80-120 μm: 0.65±0.05, 5 mice, p=0.06, Mann-Whitney U test), (P4-5, KO) (0-40 μm: 0.79±0.05; 80-120 μm: 0.63±0.08, 5 mice, p=0.09), (P9-10, Control) (0-40 μm: 0.35 ±0.05; 80-120μm: 0.20±0.05, 6 mice, p=0.13), (P9-10, KO) (0-40 μm: 0.66±0.04; 80-120 μm: 0.35±0.05, 8 mice, p=0.001). Along the rostro-caudal axis, in contrast, average correlation coefficients seemed independent of the cell separation (P4-5, Control) (0-40 μm: 0.75±0.04; 80-120 μm: 0.79±0.04, p=0.79), (P4-5, KO) (0-40 μm: 0.74±0.06; 80-120 μm: 0.72±0.02, p=1.00), (P9-10, Control) (0-40 μm: 0.28±0.05; 80-120μm: 0.34±0.05, p=0.43), (P9-10, KO) (0-40 μm: 0.54±0.04; 80-120 μm: 0.48 ± 0.05, p=0.38). The developmental desynchronization of PC activity was then evaluated individually for close (0-40 μm) and distant (80-120 μm) medio-lateral

separations in both genotypes (Fig. 9B). In control mice, the decrease of the correlation coefficient from P4-5 to P9-10 was statistically significant in both groups. (0-40μm, Control) (P4-5: 0.80±0.04, 5 mice; P9-10: 0.35±0.05, 6 mice, $p<0.01$, Mann-Whitney U test) (Fig. 9B left); (80-120μm, Control) (P4-5: 0.65±0.05; P9-10: 0.20±0.05, $p<0.01$) (Fig. 9B right). In PC-Ca_v 2.1 KO mice, there was no significant desynchronization of activity in the group of closely separated pairs, whereas the desynchronization was almost normal in the distantly separated group. (0-40μm, KO) (P4-5: 0.79 ± 0.05, 5 mice; P9-10: 0.66 ± 0.04, 8 mice $p=0.17$) (Fig. 9B left); (80-120μm, KO) (P4-5: 0.63±0.08; P9-10: 0.35±0.05, $p<0.01$) (Fig. 9B right). In summary, these data show that the developmental decorrelation of PC population activity is impaired in PC-Ca_v 2.1 KO mice. In particular, the activity in rostro-caudally oriented clusters of cells (corresponding to the group with close medio-lateral separations in the analysis above) fails to desynchronize at the end of the first postnatal week, while more medio-laterally distant pairs desynchronize almost normally. Taken together, these results suggest that the configuration of the CF network might have an impact on the pattern of PC population activity and that the progressive desynchronization of CF responses during the development could be attributed, at least in part, to the refinement of the CF network.

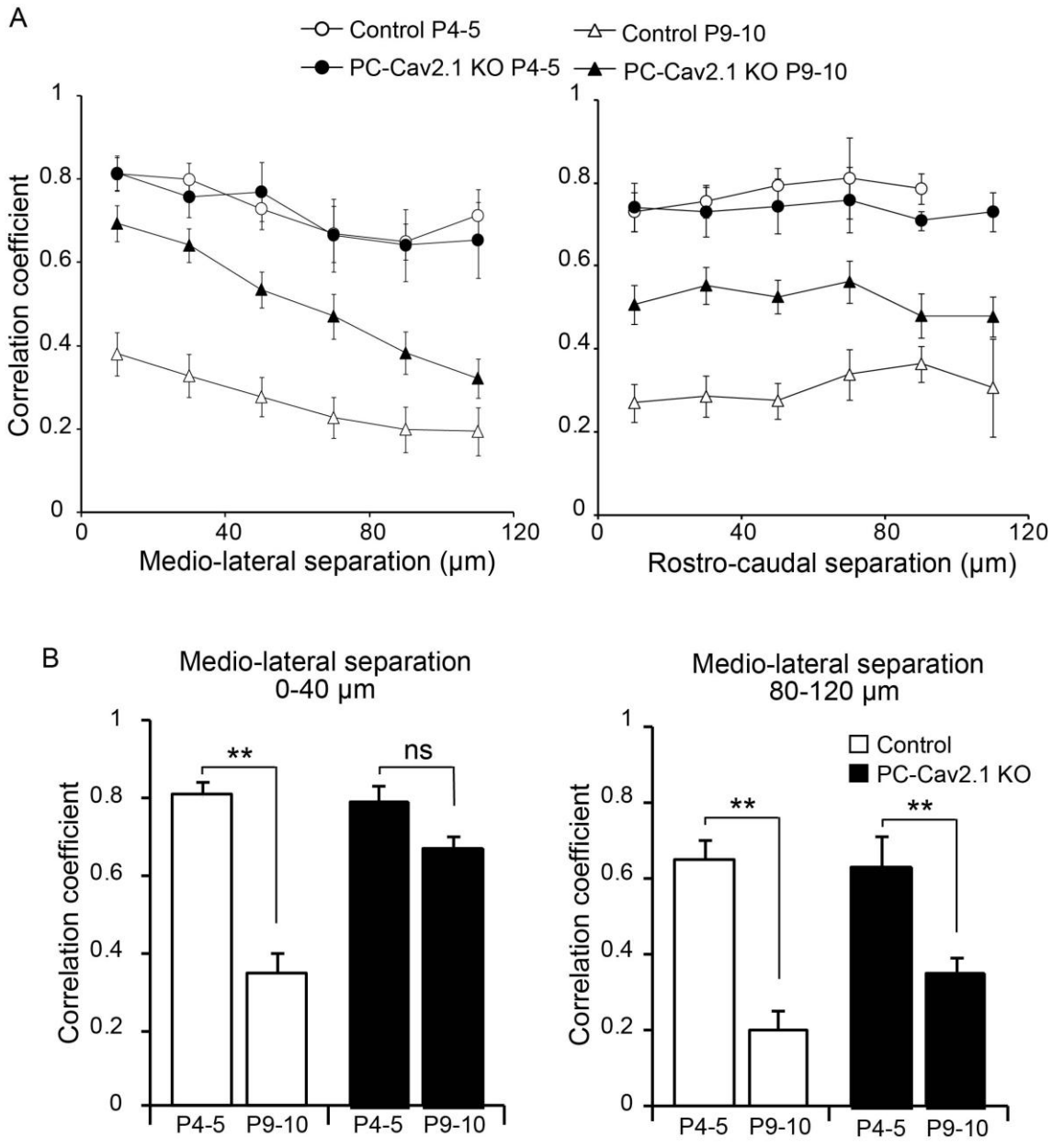

Figure 9

Impaired desynchronization of PC population activity in PC-Ca_v2.1 KO mouse.

(A) Mean correlation coefficients between pairs of deconvolved calcium transients plotted against the medio-lateral (left) and rostro-caudal (right) separation in PC-Ca_v2.1 KO and control mice during the postnatal period. Control: P4-5: 5 mice, 185 pairs; P9-10: 6 mice, 436 pairs. PC-Ca_v2.1 KO: P4-5: 5 mice, 190 pairs; P9-10: 8 mice, 722 pairs. (B) Averaged correlation coefficients in PC-Ca_v2.1 KO and control mice for cell pairs with a medio-lateral separation of 0-40µm (left) and 80-120µm (right). Asterisks demonstrate statistical significance using Mann-Whitney U test.

I next explored the mechanism by which the desynchronization of PC population activity is impaired in PC-Ca_v2.1 KO mice. One possibility is that it is due to an incomplete remodeling of the CF terminal arbors from creeper type to nest type, resulting in an abnormally wide innervation territory of single CFs. To test this hypothesis, a morphological analysis of the CF network by a triple fluorescent labeling for calbindin (PC marker), VGluT2 (CF terminal marker) and the anterograde tracer Alexa 594 (DA-594) was performed at P10 (Fig. 10). As the desynchronization was predominantly impaired along the rostro-caudal axis, this experiment was carried out in parasagittal slices. First, the horizontal length of CFs collaterals, from the bifurcation from the main branch to the terminal tip, was compared in both genotypes (Fig. 10 A1-B1). The mean value was significantly higher in the KO. Control: 13.3±1.2μm n=39 ; KO: 32.5±2.2μm n=55 p<0.0001 Mann-Whitney U test (Fig. 10C left). To check whether these branches form synapses onto PCs, the number of VGluT2 positive terminals per CF collateral was evaluated (Fig. 10 A2-B2). On average, CF collaterals in PC-Ca_v2.1 KO mice had more VGluT2 positive terminals than those in control mice. Control: 2.4±0.3 n=39; KO: 12.8±1.1 n=55 p<0.0001 (Fig. 10C right). In summary, these data show that CF collaterals along the rostro-caudal axis are longer in PC-Ca_v2.1 KO than in control. Taken together, these results provide a morphological basis for the

impaired desynchronization of CF activity in PC populations in PC-Ca_v 2.1 KO mice.

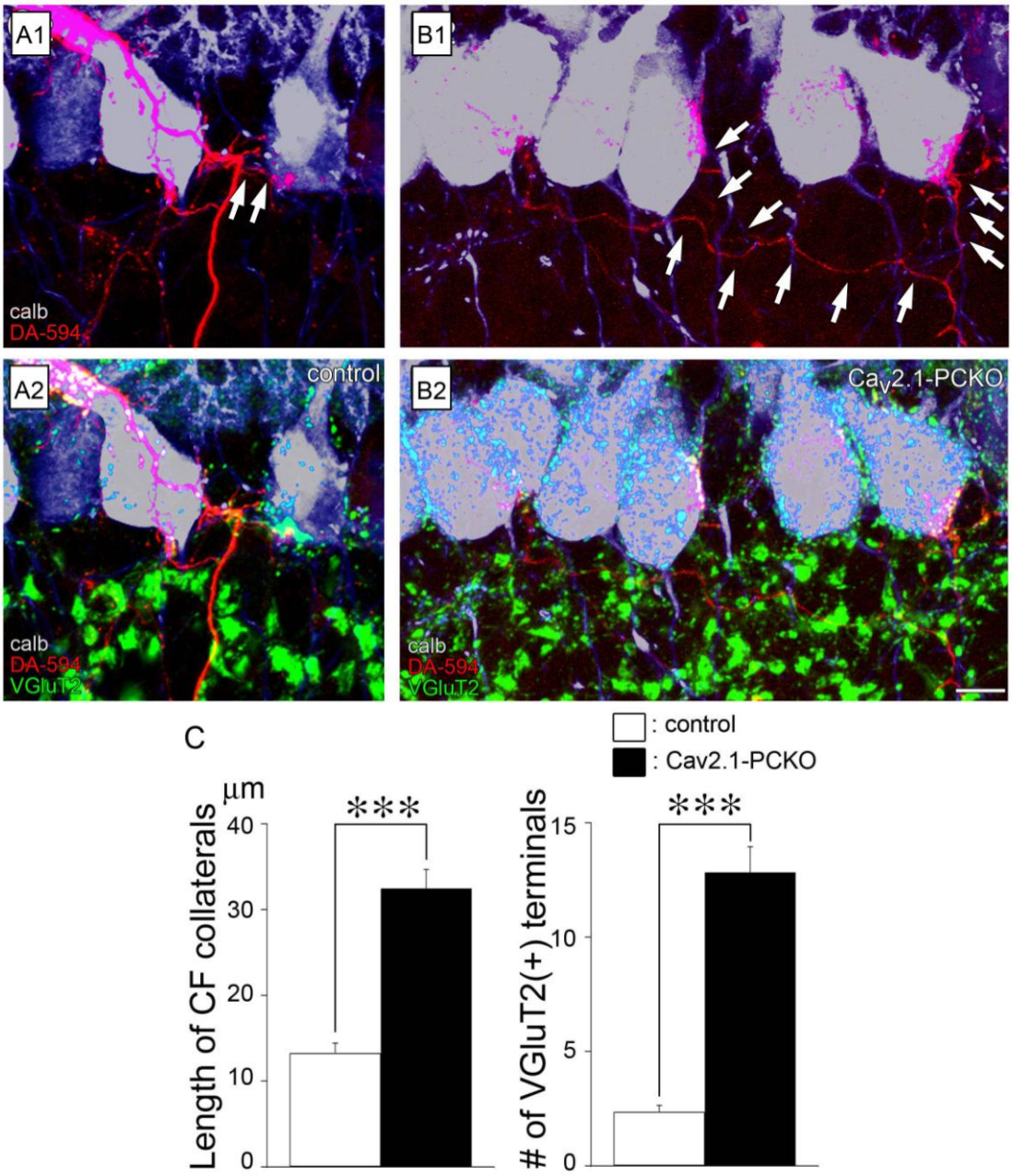

Figure 10

Impaired pruning of CF collaterals in PC-Ca_v 2.1 KO mice at P10.

(A-B) Triple fluorescent labeling for calbindin (grey), VGluT2 (green) and anterogradely labeled CFs by dextran Alexa 594 (DA-594, red) in control mice (A) and PC-Ca_v 2.1 KO (B) at P10. (A1-B1) Arrows indicate representative DA-594-labeled CF collaterals that are visible from their bifurcation from the main branches to the terminal tips on the PC soma. (A2-B2) VGluT2-positive CF terminals can be seen on PC somata and dendrites. (F) Mean horizontal length of CF collaterals (left) and number of VGluT2-positive terminals per CF collateral (right) in both genotypes. (scale bar, 10μm)

Discussion

In this study, I used *in vivo* two-photon calcium imaging to monitor CF responses from populations of PCs during the period of CF network refinement. I found that a dramatic change occurred in the spatiotemporal organization of activity over the course of development. PC population activity, which was highly correlated soon after birth, underwent a uniform desynchronization from P5. The synchrony reached the adult level approximately at P8. To gain insight into the mechanisms underlying this phenomenon, I next analyzed PC-Ca_v2.1 KO mouse, in which CF-PC synapse refinement is impaired. The desynchronization observed in the WT mouse was incomplete in the KO mouse. In particular, the activity in clusters of rostro-caudally oriented PCs remained highly correlated at P9-10. Interestingly, the morphological analysis of PC-Ca_v2.1 KO mouse revealed that CF collaterals with synaptic boutons along the rostro-caudal axis were longer than in control littermates.

The results suggest that the desynchronization of PC population activity is a consequence of the CF network refinement. One possibility is that the developmental contraction of the innervation territory during the refinement of CF terminal arbors results in a decline of synchrony. This hypothesis is supported by the fact that the two phenomena occur approximately at the same time during the development [41]. In

addition, the presence of both abnormally long CF collaterals and an incomplete desynchronization in PC-Ca_v 2.1 KO mouse is also consistent with this interpretation. The schematics of Figure 11 explain how the morphological remodeling of CF terminal arbors could lead to the spatio-temporal reorganization of the PC population activity.

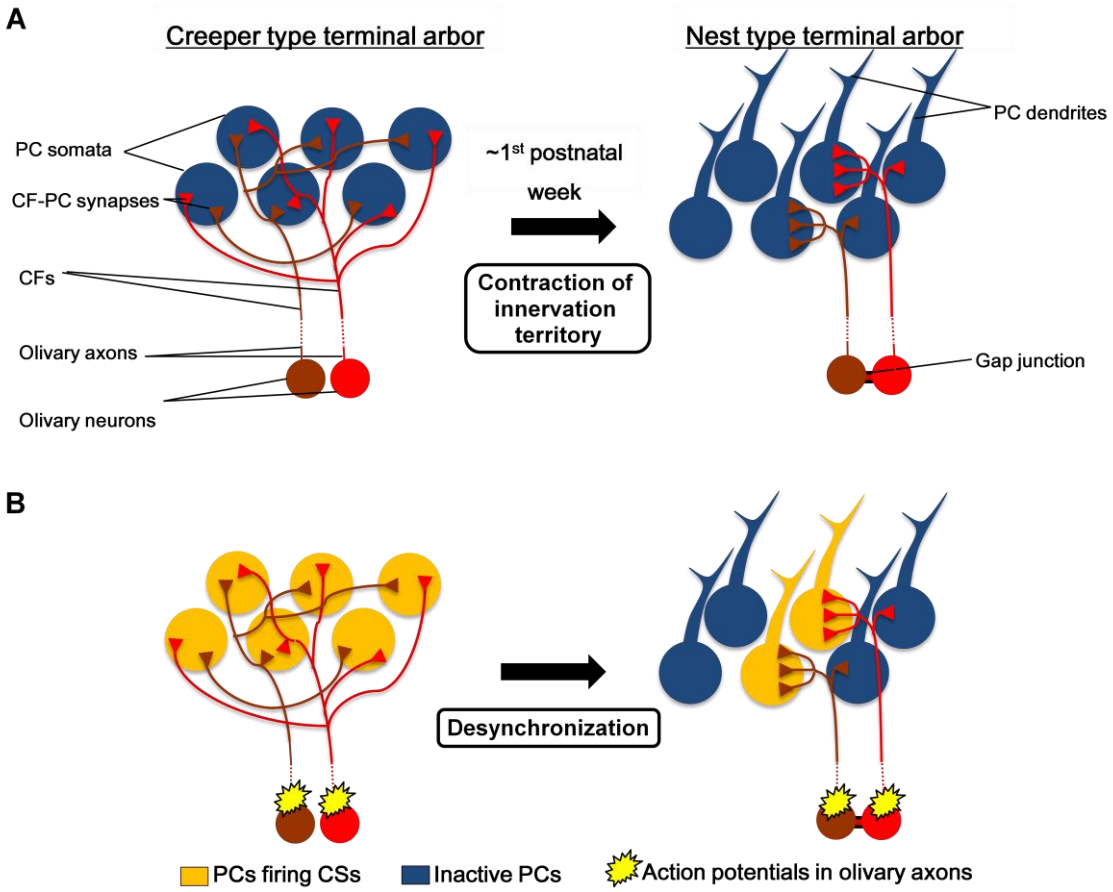

Figure 11

Postnatal refinement of CF terminal arbor and desynchronization of PC population activity.

(A) Soon after birth, each CF will make contacts with several PCs (“creeper” type terminal arbor). At the end of the first postnatal week, the innervation territory of single CFs will contract to form a “nest” type terminal arbor, characterized by a dense aggregation of terminals tightly surrounding single PC somata. (B) In the “creeper” type configuration, activation of a group of olivary neurons generates synchronized CSs in a large cluster of PCs (left). After the contraction of the innervation territory, a similar activation produces CSs in a restricted cluster of cells which results in a more independent firing and lower population synchrony (right). At this stage, the residual level of synchrony is determined by the presence of gap junctions between olivary neurons.

On the other hand, the functional differentiation of CF-PC synapse could also be involved in reshaping the pattern of population activity during the first postnatal week. Again, the fact that desynchronization and functional differentiation happen with a similar timing is consistent with this possibility. It is also concordant with the fact that, in PC-Ca_v 2.1 KO mouse, both phenomena are impaired. How would the CF-PC synapse strengthening regulate the level of synchrony? A recent report showed that, while a unique input from the strong CF is sufficient to trigger a CS after the functional differentiation, the summation of several CF inputs is required to generate a CS before the functional differentiation (unpublished data. Y. Kawamura et al. ref (Analysis of Climbing fiber inputs to Purkinje cells in the developing rat cerebellum in vivo. Kawamura, Y, Nakayama, H, Kitamura, K, Kano, M. Journal of physiological sciences vol. 59, suppl. 1, p137, 2009). Based on this finding, it is conceivable that synchronized CF inputs only are transmitted to PCs in new born animals, while more decorrelated inputs, which are not able to be summated, cannot induce sufficient depolarization of PCs to trigger CSs. This would explain why the level of synchrony in CF responses is high before synaptic strengthening. This hypothesis implicates that the level of synchrony is lower in the inferior olive than in the cerebellar cortex during early

postnatal period. Indeed, a recent report showed that population activity of olivary neuron is relatively desynchronized soon after birth and that there is no further decrease in synchrony during the first ten days of life [61].

In PC-Ca_v2.1 KO mouse, not one but several CFs are equally strengthened to a lesser extent than in WT mouse [49]. The incomplete desynchronization observed in this mouse could result from this partial strengthening. For example, if the number of inputs required for evoking CS decreases, it would be possible that more desynchronized inputs from the inferior olive are reliably transmitted. On the other hand, the incomplete desynchronization might also be due to a decrease in the innervation territory of each CF due to a halfway remodeling of its terminal arbors.

I cannot exclude that the mechanism for high synchrony and subsequent desynchronization of CF responses does not originate in the inferior olive. First, a developmental regulation of the electrical coupling between olivary neurons might be involved. However, this hypothesis seems unlikely as the expression of connexin36, the main subunit of gap junctions, is weaker at birth than in mature animals [62]. Furthermore, an ultrastructural study suggests that functional gap junctions might appear only around P10 in rat [63]. Finally, as mentioned before, population activity of olivary neurons in slices is relatively desynchronized soon after birth and does not

undergo any further decrease in synchrony during the first ten days of life [61]. Another possibility is that afferents to the inferior olive themselves are synchronized. Neocortex and spinal cord, which send afferents to the inferior olive in mature animals [64], exhibit a synchronous pattern of activity during the early postnatal period [19, 20, 65]. However, mature synapses onto olivary neurons are scarce during the first days of life [63]. Experiments monitoring population activity of inferior olivary neurons *in vivo* would help to exclude this possibility.

The significance of the immature spatio-temporal pattern of activity in the cerebellar cortex is not well understood. One possibility is that synchronized inputs during the first postnatal week promote plastic changes at CF-PC synapse through competitive Hebbian mechanisms. This hypothesis is supported by the fact that long-term potentiation (LTP) is evoked at immature CF-PC synapse when CF stimulation is paired with a postsynaptic depolarization involving calcium influx [66, 67]. In particular, this form of LTP is proposed to be involved in the functional differentiation of CF-PC synapses. However, it is not clear how only one CF-PC synapse could be selected and strengthened relatively to the others considering that the co-activation of several CF inputs are required to generate postsynaptic calcium transients. Furthermore, the functional differentiation is impaired in PC-Ca_v2.1 KO mouse despite a grossly normal

synchronous pattern of activity during the first days of life. Therefore, coordinated PC population activity is not the only prerequisite for synapse strengthening. Experiment disrupting the synchrony during the first days of life could help to gain insight into the functional significance of this specific spatio-temporal pattern of activity.

In conclusion, I monitored for the first time the cerebellar PC population activity during the early postnatal period *in vivo*. I showed that a dramatic desynchronization of CF responses occurs at the end of the first postnatal week. Then, I demonstrated how the refinement of the CF network is involved in this developmental reshaping of the population activity. These data give a new insight into the interplay between the CF network refinement and the pattern of PC population activity in the cerebellar cortex during postnatal development.

Acknowledgments

I would like to express my sincere gratitude to Professor Masanobu Kano for having accepted me as a Ph-D student and for his supervision. I also warmly thank Dr. Kazuo Kitamura for his advice, supervision and helpful discussions. Finally I am very grateful to Drs. Yuki Sugaya and Shinichiro Tsutsumi for their help about data analysis, and to Miki Hashizume for useful advice. This project was supported by a scholarship for foreign students from the Ministry of Education, Culture, Sports, Science and Technology of Japan.

References

1. Redmond, L., A.H. Kashani, and A. Ghosh, *Calcium regulation of dendritic growth via CaM kinase IV and CREB-mediated transcription.* Neuron, 34(6): p. 999-1010.2002.
2. Fueshko, S.M., S. Key, and S. Wray, *GABA inhibits migration of luteinizing hormone-releasing hormone neurons in embryonic olfactory explants.* J Neurosci, 18(7): p. 2560-9.1998.
3. Hanson, M.G. and L.T. Landmesser, *Normal patterns of spontaneous activity are required for correct motor axon guidance and the expression of specific guidance molecules.* Neuron, 43(5): p. 687-701.2004.
4. Shatz, C.J. and M.P. Stryker, *Prenatal tetrodotoxin infusion blocks segregation of retinogeniculate afferents.* Science, 242(4875): p. 87-9.1988.
5. Mostafapour, S.P., et al., *Patterns of cell death in mouse anteroventral cochlear nucleus neurons after unilateral cochlea removal.* J Comp Neurol, 426(4): p. 561-71.2000.
6. Penn, A.A., et al., *Competition in retinogeniculate patterning driven by spontaneous activity.* Science, 279(5359): p. 2108-12.1998.
7. Hong, Y.K. and C. Chen, *Wiring and rewiring of the retinogeniculate synapse.* Curr Opin Neurobiol, 21(2): p. 228-37.2011.
8. Torborg, C.L., K.A. Hansen, and M.B. Feller, *High frequency, synchronized bursting drives eye-specific segregation of retinogeniculate projections.* Nat Neurosci, 8(1): p. 72-8.2005.
9. Komuro, H. and P. Rakic, *Orchestration of neuronal migration by activity of ion channels, neurotransmitter receptors, and intracellular Ca2+ fluctuations.* J Neurobiol, 37(1): p. 110-30.1998.
10. Moody, W.J. and M.M. Bosma, *Ion channel development, spontaneous activity, and activity-dependent development in nerve and muscle cells.* Physiol Rev, 85(3): p. 883-941.2005.
11. Garaschuk, O., et al., *Large-scale oscillatory calcium waves in the immature cortex.* Nat Neurosci, 3(5): p. 452-9.2000.
12. Flint, A.C., R.S. Dammerman, and A.R. Kriegstein, *Endogenous activation of metabotropic glutamate receptors in neocortical development causes neuronal calcium oscillations.* Proc Natl Acad Sci U S A, 96(21): p. 12144-9.1999.
13. Ben-Ari, Y., et al., *Giant synaptic potentials in immature rat CA3 hippocampal neurones.* J Physiol, 416: p. 303-25.1989.
14. Garaschuk, O., E. Hanse, and A. Konnerth, *Developmental profile and synaptic*

origin of early network oscillations in the CA1 region of rat neonatal hippocampus. J Physiol, 507 (Pt 1): p. 219-36.1998.

15. Khazipov, R. and H.J. Luhmann, *Early patterns of electrical activity in the developing cerebral cortex of humans and rodents.* Trends Neurosci, 29(7): p. 414-8.2006.
16. Leinekugel, X., et al., *Ca2+ oscillations mediated by the synergistic excitatory actions of GABA(A) and NMDA receptors in the neonatal hippocampus.* Neuron, 18(2): p. 243-55.1997.
17. Milner, L.D. and L.T. Landmesser, *Cholinergic and GABAergic inputs drive patterned spontaneous motoneuron activity before target contact.* J Neurosci, 19(8): p. 3007-22.1999.
18. Wong, R.O., M. Meister, and C.J. Shatz, *Transient period of correlated bursting activity during development of the mammalian retina.* Neuron, 11(5): p. 923-38.1993.
19. Golshani, P., et al., *Internally mediated developmental desynchronization of neocortical network activity.* J Neurosci, 29(35): p. 10890-9.2009.
20. Rochefort, N.L., et al., *Sparsification of neuronal activity in the visual cortex at eye-opening.* Proc Natl Acad Sci U S A, 106(35): p. 15049-54.2009.
21. Yuste, R., A. Peinado, and L.C. Katz, *Neuronal domains in developing neocortex.* Science, 257(5070): p. 665-9.1992.
22. Dupont, E., et al., *Rapid developmental switch in the mechanisms driving early cortical columnar networks.* Nature, 439(7072): p. 79-83.2006.
23. Desclin, J.C., *Histological evidence supporting the inferior olive as the major source of cerebellar climbing fibers in the rat.* Brain Res, 77(3): p. 365-84.1974.
24. Sugihara, I., H. Wu, and Y. Shinoda, *Morphology of single olivocerebellar axons labeled with biotinylated dextran amine in the rat.* J Comp Neurol, 414(2): p. 131-48.1999.
25. Eccles, J.C., R. Llinas, and K. Sasaki, *The excitatory synaptic action of climbing fibres on the purinje cells of the cerebellum.* J Physiol, 182(2): p. 268-96.1966.
26. Kitamura, K. and M. Hausser, *Dendritic calcium signaling triggered by spontaneous and sensory-evoked climbing fiber input to cerebellar Purkinje cells in vivo.* J Neurosci, 31(30): p. 10847-58.2011.
27. Raman, I.M. and B.P. Bean, *Ionic currents underlying spontaneous action potentials in isolated cerebellar Purkinje neurons.* J Neurosci, 19(5): p. 1663-74.1999.
28. Mittmann, W. and M. Hausser, *Linking synaptic plasticity and spike output at excitatory and inhibitory synapses onto cerebellar Purkinje cells.* J Neurosci,

27(21): p. 5559-70.2007.

29. Mittmann, W., U. Koch, and M. Hausser, *Feed-forward inhibition shapes the spike output of cerebellar Purkinje cells.* J Physiol, 563(Pt 2): p. 369-78.2005.
30. Sotelo, C., R. Llinas, and R. Baker, *Structural study of inferior olivary nucleus of the cat: morphological correlates of electrotonic coupling.* J Neurophysiol, 37(3): p. 541-59.1974.
31. De Zeeuw, C.I., et al., *Association between dendritic lamellar bodies and complex spike synchrony in the olivocerebellar system.* J Neurophysiol, 77(4): p. 1747-58.1997.
32. Blenkinsop, T.A. and E.J. Lang, *Block of inferior olive gap junctional coupling decreases Purkinje cell complex spike synchrony and rhythmicity.* J Neurosci, 26(6): p. 1739-48.2006.
33. Llinas, R. and K. Sasaki, *The Functional Organization of the Olivo-Cerebellar System as Examined by Multiple Purkinje Cell Recordings.* Eur J Neurosci, 1(6): p. 587-602.1989.
34. Wylie, D.R., C.I. De Zeeuw, and J.I. Simpson, *Temporal relations of the complex spike activity of Purkinje cell pairs in the vestibulocerebellum of rabbits.* J Neurosci, 15(4): p. 2875-87.1995.
35. Ozden, I., et al., *Reliable coding emerges from coactivation of climbing fibers in microbands of cerebellar Purkinje neurons.* J Neurosci, 29(34): p. 10463-73.2009.
36. Lang, E.J., I. Sugihara, and R. Llinas, *GABAergic modulation of complex spike activity by the cerebellar nucleoolivary pathway in rat.* J Neurophysiol, 76(1): p. 255-75.1996.
37. Lang, E.J., *Organization of olivocerebellar activity in the absence of excitatory glutamatergic input.* J Neurosci, 21(5): p. 1663-75.2001.
38. Lang, E.J., *GABAergic and glutamatergic modulation of spontaneous and motor-cortex-evoked complex spike activity.* J Neurophysiol, 87(4): p. 1993-2008.2002.
39. Hashimoto, K. and M. Kano, *Functional differentiation of multiple climbing fiber inputs during synapse elimination in the developing cerebellum.* Neuron, 38(5): p. 785-96.2003.
40. Hashimoto, K., et al., *Translocation of a "winner" climbing fiber to the Purkinje cell dendrite and subsequent elimination of "losers" from the soma in developing cerebellum.* Neuron, 63(1): p. 106-18.2009.
41. Sugihara, I., *Microzonal projection and climbing fiber remodeling in single olivocerebellar axons of newborn rats at postnatal days 4-7.* J Comp Neurol,

487(1): p. 93-106.2005.

42. Chedotal, A. and C. Sotelo, *The 'creeper stage' in cerebellar climbing fiber synaptogenesis precedes the 'pericellular nest'--ultrastructural evidence with parvalbumin immunocytochemistry.* Brain Res Dev Brain Res, 76(2): p. 207-20.1993.
43. Mason, C.A., S. Christakos, and S.M. Catalano, *Early climbing fiber interactions with Purkinje cells in the postnatal mouse cerebellum.* J Comp Neurol, 297(1): p. 77-90.1990.
44. Lorenzetto, E., et al., *Genetic perturbation of postsynaptic activity regulates synapse elimination in developing cerebellum.* Proc Natl Acad Sci U S A, 106(38): p. 16475-80.2009.
45. Kano, M., et al., *Persistent multiple climbing fiber innervation of cerebellar Purkinje cells in mice lacking mGluR1*. Neuron, 18(1): p. 71-9.1997.
46. Miyazaki, T., et al., *P/Q-type Ca2+ channel alpha1A regulates synaptic competition on developing cerebellar Purkinje cells.* J Neurosci, 24(7): p. 1734-43.2004.
47. Rabacchi, S., et al., *Involvement of the N-methyl D-aspartate (NMDA) receptor in synapse elimination during cerebellar development.* Science, 256(5065): p. 1823-5.1992.
48. Kakizawa, S., et al., *Critical period for activity-dependent synapse elimination in developing cerebellum.* J Neurosci, 20(13): p. 4954-61.2000.
49. Hashimoto, K., et al., *Postsynaptic P/Q-type Ca2+ channel in Purkinje cell mediates synaptic competition and elimination in developing cerebellum.* Proc Natl Acad Sci U S A, 108(24): p. 9987-92.2011.
50. Kano, M., et al., *Impaired synapse elimination during cerebellar development in PKC gamma mutant mice.* Cell, 83(7): p. 1223-31.1995.
51. Sullivan, M.R., et al., *In vivo calcium imaging of circuit activity in cerebellar cortex.* J Neurophysiol, 94(2): p. 1636-44.2005.
52. Stosiek, C., et al., *In vivo two-photon calcium imaging of neuronal networks.* Proc Natl Acad Sci U S A, 100(12): p. 7319-24.2003.
53. Pologruto, T.A., B.L. Sabatini, and K. Svoboda, *ScanImage: flexible software for operating laser scanning microscopes.* Biomed Eng Online, 2: p. 13.2003.
54. Yaksi, E. and R.W. Friedrich, *Reconstruction of firing rate changes across neuronal populations by temporally deconvolved Ca2+ imaging.* Nat Methods, 3(5): p. 377-83.2006.
55. Louie, K. and M.A. Wilson, *Temporally structured replay of awake hippocampal ensemble activity during rapid eye movement sleep.* Neuron, 29(1): p.

145-56.2001.

56. Kitamura, K., et al., *Targeted patch-clamp recordings and single-cell electroporation of unlabeled neurons in vivo.* Nat Methods, 5(1): p. 61-7.2008.
57. Miyazaki, T. and M. Watanabe, *Development of an anatomical technique for visualizing the mode of climbing fiber innervation in Purkinje cells and its application to mutant mice lacking GluRdelta2 and Ca(v)2.1.* Anat Sci Int, 86(1): p. 10-8.2011.
58. Miura, E., et al., *Expression and distribution of JNK/SAPK-associated scaffold protein JSAP1 in developing and adult mouse brain.* J Neurochem, 97(5): p. 1431-46.2006.
59. Miyazaki, T., et al., *Subtype switching of vesicular glutamate transporters at parallel fibre-Purkinje cell synapses in developing mouse cerebellum.* Eur J Neurosci, 17(12): p. 2563-72.2003.
60. Schultz, S.R., et al., *Spatial pattern coding of sensory information by climbing fiber-evoked calcium signals in networks of neighboring cerebellar Purkinje cells.* J Neurosci, 29(25): p. 8005-15.2009.
61. Rekling, J.C., K.H. Jensen, and H. Jahnsen, *Spontaneous cluster activity in the inferior olivary nucleus in brainstem slices from postnatal mice.* J Physiol, 590(Pt 7): p. 1547-62.2012.
62. Van Der Giessen, R.S., et al., *Spatiotemporal distribution of Connexin45 in the olivocerebellar system.* J Comp Neurol, 495(2): p. 173-84.2006.
63. Bourrat, F. and C. Sotelo, *Postnatal development of the inferior olivary complex in the rat. I. An electron microscopic study of the medial accessory olive.* Brain Res, 284(2-3): p. 291-310.1983.
64. De Zeeuw, C.I., et al., *Microcircuitry and function of the inferior olive.* Trends Neurosci, 21(9): p. 391-400.1998.
65. Whelan, P., A. Bonnot, and M.J. O'Donovan, *Properties of rhythmic activity generated by the isolated spinal cord of the neonatal mouse.* J Neurophysiol, 84(6): p. 2821-33.2000.
66. Bosman, L.W., et al., *Homosynaptic long-term synaptic potentiation of the "winner" climbing fiber synapse in developing Purkinje cells.* J Neurosci, 28(4): p. 798-807.2008.
67. Ohtsuki, G. and T. Hirano, *Bidirectional plasticity at developing climbing fiber-Purkinje neuron synapses.* Eur J Neurosci, 28(12): p. 2393-400.2008.